AIAA JOURNAL
Vol. 46, No. 5, May 2008

Nonpremixed Combustion in an Accelerating Turning Transonic Flow Undergoing Transition

Felix Cheng,* Feng Liu,† and William A. Sirignano‡
University of California, Irvine, California 92697-3975

DOI: 10.2514/1.35209

Mixing layers composed of gaseous fuel and oxidizer streams passing through curved channels with or without chemical reactions are studied by performing two-dimensional numerical simulations. The flows are subjected to either transverse acceleration or both transverse and streamwise accelerations; the flow accelerates from low subsonic speed to low supersonic speed in the case with the streamwise acceleration. We focus on the development of the mixing layers from laminar flow to the transition regime. The full Navier–Stokes equations coupled with multiple-species equations and the energy equations with chemical reactions are solved using a finite-difference numerical scheme. The effects of turning are investigated on two different flow configurations; one has a faster and lighter air stream on the outside of the curve and a slower and heavier fuel stream on the inside of the curve, the other one has a slower and heavier fuel stream on the outside of the curve and a faster and lighter air stream on the inside of the curve. Because of the turning, the flow profiles are significantly altered, and the instability mechanisms are modified. In most cases, the mixing layers with the faster and lighter air stream on the outside are more unstable than the mixing layers with the heavier and slower fuel stream on the outside. The reacting mixing layers are always more unstable than the corresponding nonreacting cases in terms of the turbulent kinetic energy. Positive and negative vorticities are generated in the reacting case by the baroclinic effect associated with the large density gradient across the combustion zone. The mixing layers with imposed streamwise accelerations show stabilizing effects, and the chemical conversion rates decrease due to the acceleration.

I. Introduction

DESIGNERS of jet engines are attempting to increase the thrust-to-weight ratio and to widen the range of engine operation. Because the flow in a turbine passage is accelerating and power is extracted from the flow, it is possible to add heat without increasing the flow temperature beyond the turbine-blade material limit. Sirignano and Liu [1,2] show by thermodynamic analysis that the thrust of aircraft turbojet and turbofan engines can be increased significantly with little increase in fuel consumption by intentionally burning fuel in the turbine stages. For the ground-based gas turbine, improvement has been found in power/weight and efficiencies [1]. Mixing and exothermic chemical reactions in the accelerating flow through the turbine passage offer an opportunity for a major technological improvement. The gas turbine engine is not the only potential application for this technology. The reduction in peak temperature due to acceleration results in the promise of reduced pollutant formation and reduced heat transfer loss in many other combustion applications.

The geometry of the turbine passage is rather complex. To simplify the problem while retaining the major physics in the present study, we create a model problem in this paper in which a mixing layer of fuel and oxidizer streams going through a curved channel with or without imposed streamwise pressure gradients is studied. Both nonreacting and reacting mixing layers are considered in this paper. The nonreacting cases primarily serve as the base cases; the main focus is on the reacting mixing layers. Note that we are not performing numerical simulations on the actual flows in a turbine passage; instead, we focus on the fundamental physics, such as the effects of streamwise and transverse accelerations on the instability and the chemical reactions in the reacting, accelerating mixing layers.

There has been little previous research on steady-state multidimensional flows with mixing and chemical reactions in the presence of strong pressure gradients. Research has been done on high-speed, nonaccelerating, reacting flows. A comprehensive literature review was done by Sirignano and Kim [3]. In that paper, they also obtained similarity solutions for laminar, two-dimensional, mixing, reacting, and nonreacting layers with a favorable pressure gradient in the primary flow direction. Fang et al. [4] extended that study to mixing layers with arbitrary pressure gradients by using a finite-difference method for the boundary-layer equations. The influence of the pressure gradient, initial temperature, initial pressure, initial velocity, and transport properties was studied. Mehring et al. [5] performed a numerical study on a reacting, turbulent, and accelerating mixing layer based on the laminar boundary-layer calculations by Fang et al. [4]. Cai et al. [6] developed a finite-volume method for solving the two-dimensional, compressible, Favre-averaged Navier–Stokes equations with chemical reactions using the Baldwin–Lomax turbulence model.

The steady-state calculations provide important insight into the fundamental physics of multidimensional mixing layers with chemical reactions and strong pressure gradients. However, they are unable to capture the unsteady developments in which the flows evolve from laminar conditions to turbulence. Motivated by this, the primary objective of this paper is to investigate the initial developments of the two-dimensional, reacting, accelerating mixing layers from the laminar stage to the early transitional stage.

The nonreacting mixing layers going through the curved channel are subjected to three types of instability; they are the Kelvin–Helmholtz (KH), centrifugal, and Rayleigh–Taylor (RT) instabilities. KH instability occurs in a shear layer; it has been studied extensively in experiments, stability analyses, and numerical analyses (see Ho and Huerre [7]). For a planar shear layer, the 2-D KH modes are more unstable than the 3-D modes in the linear stage or in the early stage of transition. Experimental studies by Winant and Browand [8] show that, at the early stage of transition, the

Received 18 October 2007; revision received 5 January 2008; accepted for publication 14 January 2008.

*Graduate Student Researcher, Department of Mechanical and Aerospace Engineering. Member AIAA.
†Professor, Department of Mechanical and Aerospace Engineering. Associate Fellow AIAA.
‡Professor, Department of Mechanical and Aerospace Engineering. Fellow AIAA.

development of the mixing layer is dominated by large-scale, two-dimensional spanwise vortices that arise from the KH instability. In highly turbulent mixing layers, the development of the three-dimensional streamwise vortices become significant. Numerical simulations of three-dimensional temporally evolving plane mixing layers were performed by Moser and Rogers [9,10]. Infinitesimal three-dimensional disturbances were imposed initially. Spanwise vorticity rolled up into corrugated spanwise rollers, and predominantly streamwise rib vortices developed in the braid region between the spanwise rollers. The development of three-dimensionality, the nonlinear evolution of three-dimensional disturbances with spanwise vortices during pairings, and the transition mechanisms were studied in detail. Although the development of three-dimensional structures is absent in our two-dimensional study, we focus on the early stages of transition in which the development of the mixing layer is dominated by the 2-D mechanism, so that our 2-D simulations will be able to capture the important physics.

Centrifugal instability [11] occurs in a curved shear layer and is caused by the centrifugal force. Depending on the velocity distribution across the curved shear layer, the centrifugal force could have a stabilizing or destabilizing effect. For an inviscid swirling flow, Rayleigh found that a necessary and sufficient condition for stability to axisymmetric disturbances is that the square of the circulation does not decrease with an increasing radius anywhere. For an unstable curved shear layer (such as a shear layer with fast fluid on the inside of the curve), a 3-D unstable mode associated with the centrifugal instability emerges. This 3-D mode induces streamwise vortices and can become the most unstable mode. RT instability can exist in a flow with acceleration when density gradients are present. It can be caused by a body force (such as gravity force). In a situation in which body force is absent, RT instability could exist in a curved flow with a density gradient. In our flow with negligible gravity force, the centrifugal force acts like "pseudogravity" and could induce RT instability. For the two-dimensional shear layers considered in this paper, the centrifugal and RT instabilities could coexist. Although both the centrifugal and RT instabilities could produce three-dimensional unstable structures, some of the important effects due to the centrifugal force are still present in the two-dimensional flows. The linear analysis performed by Liou [12] demonstrated that the centrifugal force could enhance or suppress the KH mode in a two-dimensional curved shear layer with constant density. Zhuang [13] included the effects of a density gradient in a curved shear layer and showed modifications of the KH mode. In this paper, we consider only two-dimensional curved flows; the effects of three-dimensionality are beyond the scope of this paper.

In reacting mixing layers, the stability characteristics could be different from those in nonreacting mixing layers due to the modifications of the flow profiles caused by the chemical reactions. The effects of heat release on the instability of straight, reacting mixing layers were studied by Shin and Ferziger [14] using linear stability theory. An inviscid, low-Mach-number stability equation was derived and solved numerically. With a sufficient amount of heat release, multiple unstable modes (referred to as the outer modes) in addition to the central mode (the unstable mode associated with the central inflection point of the mean-velocity profile) were found. The outer modes arose due to the modifications of the density and velocity profiles caused by the chemical reactions and were quite insensitive to the further increases in heat release. The central modes were suppressed significantly by the further increases in heat release so that the outer modes could become the dominant unstable modes. Shin and Ferziger [15] extended their previous work to include the effects of high Mach numbers. Multiple supersonic unstable modes were found in both the nonreacting and reacting flows when the phase velocity of the disturbance was supersonic relative to the freestream. The supersonic modes became less unstable with an increasing Mach number but more unstable with an increasing heat release. These modes did not seem to enhance the mixing of the two streams.

Although both nonreacting and reacting straight mixing layers have been studied extensively, curved reacting mixing layers with streamwise acceleration have received far less attention. In streamwise-accelerating curved mixing layers, centrifugal and RT instabilities could modify the central (KH) and outer (due to chemical reactions) modes and could either destabilize or stabilize the flows, for which the streamwise acceleration has a potentially stabilizing effect. A study by Cheng et al. [16] on straight mixing layers showed that the streamwise acceleration stabilized both nonreacting and reacting mixing layers. The goal of this paper is to investigate the combined effects of chemical reactions, transverse and streamwise accelerations, on the development of curved mixing layers with nonuniform density. The Navier–Stokes equations coupled with multiple-species equations and chemical source terms are solved using a finite-difference algorithm; two-dimensional numerical simulations are performed. The discussions of the governing equations and numerical scheme are presented in Sec. II. The boundary conditions are given in Sec. III. The curved nonreacting cases without imposed streamwise acceleration are presented in Sec. IV.A, whereas the curved reacting cases are discussed in Sec. IV.B. The curved nonreacting mixing layers with imposed streamwise acceleration are presented in Sec. IV.C, and the curved reacting and streamwise-accelerating mixing layers are presented in Sec. IV.D. The concluding remarks are given in Sec. V.

II. Governing Equations and Numerical Method

The flow within a turbine-blade row is high speed and often transonic. There are gradients of pressure, density, and velocity in the flowfield in both the streamwise and transverse directions. Because the geometry of the turbine passage is rather complex, in this paper we simplify the physical problem to a simulation of a mixing layer passing through a curved channel. For this simplified geometry, the effects of the streamwise acceleration and transverse acceleration are retained. Because we only consider flows evolving from the laminar stage to transitional stage, and the dominant instability is primarily two-dimensional in transition, the effects of three-dimensionality are neglected as an approximation. Also, the small-scale turbulent structures are not resolved due to the limitations in grid resolution.

The geometry of the computational domain and the flow configuration are shown in Fig. 1. The top figure shows the side view of the channel on the x–y plane, and the bottom figure shows the converging and diverging channel width on the z plane. The planar mixing layer enters the channel from the left through the inlet plane. The air and fuel streams can be placed on either the inside or the outside of the curve. Streamwise acceleration of the mixing layer is

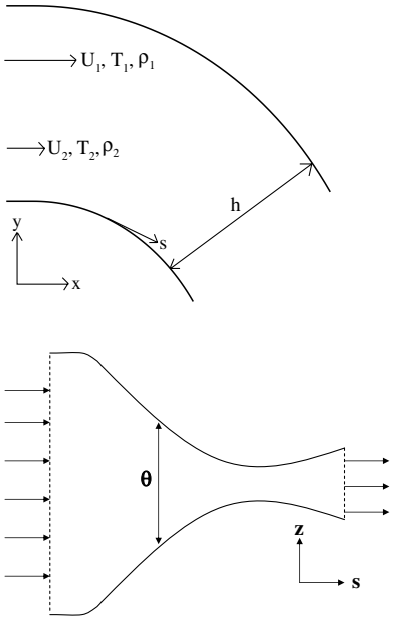

Fig. 1 Top and side views of the curved, converging–diverging channel.

achieved by contracting and expanding the channel width θ in the z direction. Because the flow is two-dimensional, there is no variation of flow properties in the spanwise (z) direction, and so θ only serves to impose streamwise pressure gradients to the flowfield. θ varies in the streamwise direction only, and it is designed in such a way that the mixing layer will be choked for the given inlet conditions and back pressure. For the nonaccelerating cases, θ is constant throughout the channel.

The governing equations, with the channel width incorporated, are the two-dimensional, compressible, multicomponent, modified Navier–Stokes equations with chemical source terms. There are a total of eight governing equations. They are the continuity equation for the total mass density, the momentum equations in the x and y directions, the energy equation, and the continuity equations for the individual mass densities of O_2, CH_4, H_2O, and CO_2. Perfect gas is assumed. The equations written in conservation form are as follows:

$$\frac{\partial \theta \mathbf{w}}{\partial t} + \frac{\partial \theta \mathbf{f}}{\partial x} + \frac{\partial \theta \mathbf{g}}{\partial g} - \frac{\partial \theta \mathbf{f}_\mu}{\partial x} - \frac{\partial \theta \mathbf{g}_\mu}{\partial y} = \theta \mathbf{s} \tag{1}$$

where $\mathbf{w}$ is the vector of the conservative variables of mass, momentum, and energy; the vectors $\mathbf{f}$ and $\mathbf{g}$ are the inviscid fluxes; $\mathbf{f}_\mu$ and $\mathbf{g}_\mu$ are the viscous fluxes; and $\mathbf{s}$ is the source term. These terms are given as

$$\mathbf{w} = \begin{pmatrix} \rho \\ \rho u \\ \rho v \\ \rho E \\ \rho_n \end{pmatrix}, \qquad \mathbf{s} = \begin{pmatrix} 0 \\ \frac{p}{\theta}\frac{\partial \theta}{\partial x} \\ \frac{p}{\theta}\frac{\partial \theta}{\partial y} \\ \dot{Q} \\ \dot{\omega}_n \end{pmatrix} \tag{2}$$

$$\mathbf{f} = \begin{pmatrix} \rho u \\ \rho u u + p \\ \rho v u \\ \rho H u \\ \rho_n u \end{pmatrix}, \qquad \mathbf{g} = \begin{pmatrix} \rho v \\ \rho u v \\ \rho v v + p \\ \rho H v \\ \rho_n v \end{pmatrix} \tag{3}$$

$$\mathbf{f}_\mu = \begin{pmatrix} 0 \\ \tau_{xx} \\ \tau_{yx} \\ u\tau_{xx} + v\tau_{yx} - q_x - \sum_{n=1}^{N} \rho_n u_{dn} h_n \\ -\rho_n u_{dn} \end{pmatrix} \tag{4}$$

$$\mathbf{g}_\mu = \begin{pmatrix} 0 \\ \tau_{xy} \\ \tau_{yy} \\ u\tau_{xy} + v\tau_{yy} - q_y - \sum_{n=1}^{N} \rho_n v_{dn} h_n \\ -\rho_n v_{dn} \end{pmatrix} \tag{5}$$

In these equations, t is time; ρ_n is density for species n, where $1 \le n \le N$ and N is the total number of species; p is pressure; μ is molecular viscosity; and u and v are the flow velocity components in the x and y directions, respectively. Other quantities are defined in the following equations:

$$\tau_{ij} = 2\mu\left[\frac{1}{2}\left(\frac{\partial u_i}{\partial x_j} + \frac{\partial u_j}{\partial x_i}\right) - \frac{1}{3}\frac{\partial u_k}{\partial x_k}\delta_{ij}\right] \tag{6}$$

$$q_j = -C_p \frac{\mu}{Pr}\frac{\partial T}{\partial x_j} \tag{7}$$

$$h = \sum_{n=1}^{N} Y_n h_n, \quad \text{and} \quad h_n = \int_{T_0}^{T} C_{pn}\, \mathrm{d}T \tag{8}$$

$$H = h + \tfrac{1}{2}(u^2 + v^2) \tag{9}$$

$$E = H - \frac{p}{\rho} \tag{10}$$

$$\dot{Q} = -\sum_{n=1}^{N} \dot{\omega}_n h_n^0 \tag{11}$$

$$\rho_n \mathbf{V}_{dn} = -\rho D_n \nabla\left(\frac{\rho_n}{\rho}\right) = -\rho D_n \nabla Y_n \tag{12}$$

where τ_{ij} is the viscous stress tensor. In these equations, the standard tensor notation is used. The subscript indices i and j take either value 1 or 2 to represent the x and y components, respectively. h_n^0 is the heat of formation of species n at the reference temperature T_0, C_{pn} is the specific heat at constant pressure of species n, $\mathbf{V}_{dn} = (u_{dn}, v_{dn})$ is the diffusion velocity of species n, and D_n is the diffusion coefficient. Because we assume unity Schmidt number and Prandtl number, $D_n = \mu/\rho$ for all species. C_{pn} and h_n vary with temperature; they are given by NASA polynomials.

Methane (CH_4) is used for the current computations although the method is not restricted to only one type of fuel. The combustion process is described by a one-step overall chemical reaction as follows:

$$C\,H_4 + 2O_2 + 7.52N_2 \longrightarrow CO_2 + 2H_2O + 7.52N_2$$

The chemical kinetics rate for the fuel is

$$\dot{\omega}_F = -W_F A e^{-E_a/RT}[\text{Fuel}]^a[O_2]^b \tag{13}$$

where the brackets [ ] represent molar concentration in mol/cm^3 and W_F is the molecular weight of fuel. For methane (CH_4), the parameter values [17] are $A = 2.8 \times 10^9$ 1/sec, $E_a =$ 48.4 kcal/mol, $a = -0.3$, and $b = 1.3$.

In the solution procedure, the average gas constant R, molecular weight W, and viscosity coefficient μ can be obtained by the following equations:

$$R = \sum_{n=1}^{N} R_n Y_n \tag{14}$$

$$\frac{1}{W} = \sum_{n=1}^{N} \frac{1}{W_n} Y_n \tag{15}$$

$$\mu = \sum_{n=1}^{N} \mu_n(T) Y_n \tag{16}$$

The molecular viscosity coefficient of each species μ_n is obtained [18] by using the Sutherland law:

$$\frac{\mu_n}{\mu_{0n}} = \left(\frac{T}{T_0}\right)^{\frac{3}{2}} \frac{T_0 + 110}{T + 110} \tag{17}$$

where T_0 is the reference temperature (298.15 K), and μ_{0n} is the reference viscosity evaluated at T_0.

Before discretization, Eq. (1) in the physical domain is transformed to a uniform computational domain by the following transformation relations:

$$\xi = \xi(x, y) \Leftrightarrow x = x(\xi, \eta) \tag{18}$$

$$\eta = \eta(x, y) \Leftrightarrow y = y(\xi, \eta) \tag{19}$$

The transformed governing equation in the computational domain is written as follows:

$$\frac{\partial(\theta \hat{\mathbf{w}})}{\partial t} + \frac{\partial(\theta \hat{\mathbf{f}})}{\partial \xi} + \frac{\partial(\theta \hat{\mathbf{g}})}{\partial \eta} - \frac{\partial(\theta \hat{\mathbf{f}}_\mu)}{\partial \xi} - \frac{\partial(\theta \hat{\mathbf{g}}_\mu)}{\partial \eta} = \frac{\theta \mathbf{s}}{J} \tag{20}$$

where $\hat{\mathbf{w}} = \mathbf{w}/J$, $\hat{\mathbf{f}} = (\xi_x \mathbf{f} + \xi_y \mathbf{g})/J$, $\hat{\mathbf{g}} = (\eta_x \mathbf{f} + \eta_y \mathbf{g})/J$, $\hat{\mathbf{f}}_\mu = (\xi_x \mathbf{f}_\mu + \xi_y \mathbf{g}_\mu)/J$, $\hat{\mathbf{g}}_\mu = (\eta_x \mathbf{f}_\mu + \eta_y \mathbf{g}_\mu)/J$, and J is the Jacobian of the grid transformation. ξ and η form a generalized coordinate system and they need not be orthogonal to each other. The definition of and method to calculate the transformation metrics ξ_x, ξ_y, η_x, η_y, and J can be found in Tannehill et al. [19]. The transformation was employed for the ease of treating curved walls and/or nonuniform meshes. Here, only nonuniform Cartesian meshes are used.

A flux-splitting algorithm similar to Steger and Warming [20] is used for spatial discretization of the inviscid flux. The inviscid flux is split into positive and negative parts according to the signs of the local eigenvalues of the flux Jacobian. A second-order upwind algorithm applied to the split inviscid fluxes yielded overshoots across the mixing layer and caused nonphysical distribution in the species mass fractions. To suppress the overshoots, a second-order upwind total-variation-diminishing (TVD) scheme [21] is employed; the Van Leer limiter satisfying the TVD conditions [21] is implemented in evaluating the derivatives of the split inviscid fluxes. Second-order central differencing is used for the viscous flux and a second-order Runge–Kutta multistage scheme is implemented for time marching. Note that, because an explicit time-marching scheme is used, the size of the time step is limited by the very small grid size at the center of the channel rather than the chemical source terms.

The numerical scheme has been tested against flows with known analytic solutions. Simulations of unsteady shock propagations show excellent agreement with the analytic solutions and excellent shock-capturing capability. Viscous diffusion was also tested by simulating an impulsive motion of a flat plate, and the exact transient solution was recovered. Steady-state solutions for a laminar, accelerating, and reacting mixing layer were compared with the solutions obtained by Cai et al. [6], and excellent agreement was obtained. The numerical simulations of a two-dimensional, nonreacting mixing layer in a straight channel were compared with a numerical study by Davis and Moore [22]. In our simulations, the freestream velocity ratio was the same as the one used in their paper. Forced disturbances were used to excite the mixing layer, and the pairing and merging of vortices were triggered by the subharmonic frequencies. The study focused on the effects of the fundamental frequency with its subharmonics on the vortex dynamics. We found that the vortex-merging patterns, the number of vortices involved in each merging, and the locations at which vortex merging occurred agreed very well with the results obtained by Davis and Moore.

III. Boundary Conditions

There are four boundaries in the computational domain; they are the inlet, exit, and upper and lower walls. Values of the conservative variable w and other physical properties must be known at the boundaries at each time step for the closure of the finite-difference equations. For simplicity, inviscid boundary conditions are applied on all boundaries.

A. Inlet Conditions

At the inlet, the density, streamwise velocity, and the mass fractions are specified as hyperbolic-tangent functions and the cross stream velocity is set to zero. For example, u is specified as follows:

$$u(y) = \bar{U}\left[1 + \lambda \tanh\left(\frac{y}{2\delta_\theta}\right)\right] \tag{21}$$

where $\lambda \equiv (U_1 - U_2)/(U_1 + U_2)$, $\bar{U} \equiv (U_1 + U_2)/2$, and δ_θ is a reference value which is a measure of the mixing-layer thickness at the inlet; δ_θ has a value of 0.000125 m in all cases. The density and mass fractions of O_2 and CH_4 are specified in the same manner. The mass fraction of N_2 is equal to $1 - Y_{O_2} - Y_{CH_4}$. To reduce reflections of waves at the inlet, the local one-dimensional characteristic equations are solved [23,24] at the inlet for pressure. With this formulation, pressure waves coming from the interior can pass through the inlet plane. The temperature of the mixing layer is calculated from the perfect gas relation using the updated pressure. Because the fractional change in pressure is very small in the freestream, the freestream temperature remains approximately constant, and the temperature profile appears similar to a hyperbolic-tangent distribution. Other nonspecified quantities can be calculated by thermodynamic relations accordingly.

B. Exit Conditions

For the cases without imposed streamwise pressure gradients, the Mach number at the exit is less than 1; therefore, one physical condition at the exit plane must be specified to maintain uniqueness and well-posedness. At the exit plane, the average value of pressure across the vertical or radial direction is specified. This allows a nonuniform distribution of pressure at the exit plane. To find the remaining variables and to allow passage of waves at the exit, we follow the common practice [25] and set the 1-D Lagrangian derivatives for ρ_i, ρu, and ρv to zero. For the cases with imposed streamwise pressure gradients, the flows achieve supersonic speed at the exit; therefore, extrapolation of variables from the interior is applied at the exit plane.

C. Side-Wall Conditions

For all cases, the side walls are treated as inviscid and impermeable. Slip conditions are applied at the walls, the normal component of velocity is zero at the walls, and the temperature gradient in the normal direction is set to zero. The study is aimed at examining the effects of mixing and reaction, and so it would be inefficient to commit resources to the resolution of boundary layers on the side walls.

IV. Computational Results

Mixing layers undergoing transition exhibit early development of large coherent structures. In this paper, our main objective is to study the transitional stage of accelerating and chemically reacting mixing layers. For all of the mixing layers considered in this paper, the onset of instability occurs naturally as the flow evolves downstream, and forced disturbances are not required for the instability to be sustained.

In this paper, two-dimensional numerical simulations have been performed. Although the three-dimensional structures associated with the centrifugal instability and Rayleigh–Taylor instability are not resolved, the effects of the centrifugal instability and Rayleigh–Taylor instability on the 2-D flows are still present, as shown by Liou [12] and Zhuang [13] with linear stability analyses.

The computational domain is the curved channel shown in Fig. 1. The channel starts with a short straight section of a length of 0.01 m and then it starts to curve. The upper and the lower curves are concentric arcs with radii of 0.13 and 0.07 m, respectively. The total turning angle is 1 rad. The length (l) of the centerline of the channel is 0.11 m or $880\delta_\theta$, and the height (h) is 0.06 m or $480\delta_\theta$, where $\delta_\theta = 0.000125$ m. The chosen computational domain is the physical domain of interest. In the present paper, we are performing numerical simulations on a wall-bounded channel with finite dimensions rather than an infinite domain. A total of 961 and 641 grid points are placed in the streamwise and transverse directions, respectively. The grid lines in the streamwise and transverse directions are parallel and perpendicular to the curved walls, respectively. In the streamwise direction, finer grid points are placed near the inlet and the grid points are stretched with increasing downstream distance. The grid sizes along the centerline range from 9.6×10^{-5} to 1.28×10^{-4} m. In the transverse direction, uniformly distributed fine grid points are placed in the middle one-third portion of the channel. This fine-grid region is large enough to cover the mixing region so that the large coherent structures can be uniformly resolved; hence, the development of the mixing layer can be captured more accurately. The grid size (in the transverse direction) in the uniform region is 4.0×10^{-5} m, and the initial mixing-layer thickness is 48 times as large as the grid size. The grid points are stretched beyond the uniform region and reach a maximum size of 7.2×10^{-4} m at the side walls. In the previous

study of the straight reacting mixing layers by Cheng et al. [16], a grid of 481×361 was used. The grid-independence studies showed that good qualitative accuracy was obtained by the 481×361 grid. In the present paper, the grid resolution is further improved by using the 961×641 grid.

Both curved and straight mixing layers are studied in this paper. The main focus is on the curved mixing layers; the results for the straight mixing layers (on a 961×641 grid) mainly serve as the base cases for comparisons. For all cases, the densities of air and fuel are 2.19 and 6.67 $\mathrm{kg/m^3}$, respectively. The initial pressure at the inlet is 10.26 atm. Because the pressure in the channel will be smaller than the inlet pressure, which is below the critical pressure of all species, no supercritical effects need to be considered. The streamwise acceleration a_s is calculated by the change in velocity (averaged for the two streams) and the residence time based on the centerline length and the average velocity of the two streams. The centrifugal acceleration (a_r) is calculated using the average of the two freestream velocities and the radius of the centerline for the channel.

The flow conditions for the straight cases are summarized in Table 1; the discussions of the straight mixing layers can be found in Cheng et al. [16] and will not be repeated here. For the curved mixing layers, two flow configurations are of particular interest because of their closer resemblance to the practical flows in the conceptual turbine burner. The first flow configuration consists of a faster and hotter air stream on the outside of the curve and a slower and colder fuel stream on the inside of the curve. The second one is the reciprocal of the first one in which a faster and hotter air stream is placed on the inside of the curve and a slower and colder fuel stream is placed on the outside of the curve. For convenience, we identify the first flow configuration as either NFL or RFL, for which the first letter designates nonreacting or reacting, the second letter designates faster or slower fluid on the outside of the curve, and the third letter designates lighter or heavier fluid on the outside of the curve. Similarly, the second flow configuration is described either as NSH or RSH. The flow conditions for the curved mixing layers are summarized in Table 2. For all cases, the Reynolds numbers at the inlet (calculated from ΔU, δ_θ, and the mean viscosity) are 415. The inlet velocity deficit defined as

$$\frac{U_{\mathrm{air}} - U_{\mathrm{fuel}}}{U_{\mathrm{air}}}$$

is 0.5 and the inlet temperature deficit defined as

$$\frac{T_{\mathrm{air}} - T_{\mathrm{fuel}}}{T_{\mathrm{air}}}$$

is 0.82. In the present paper, we are not performing parametric studies by varying the freestream variables; rather, we focus on the effects from variations of the flow configurations.

For all cases, a Courant–Friedrichs–Lewy (CFL) number of 0.5 is used, and virtually identical results are obtained with smaller CFL numbers. The nonreacting mixing layers without imposed streamwise acceleration are discussed in Sec. IV.A, the reacting mixing layers without imposed streamwise acceleration are discussed in Sec. IV.B, and the nonreacting and reacting mixing layers with imposed streamwise acceleration are discussed in Secs. IV.C and IV.D, respectively.

A. Nonreacting Mixing Layers in a Curved Channel

Nonreacting, curved mixing layers without imposed streamwise pressure gradient are investigated in this section. The NFL and NSH cases are both unstable. Similar to the straight mixing layer, the developments of the mixing layers for these cases are dominated by large coherent structures. The instantaneous contours of vorticity at 2.3 residence times for the NFL and NSH cases are shown in Figs. 2 and 3, respectively. The flow patterns for both cases are not precisely periodic in time, that is, the instantaneous vorticity fields appear similar at different times but the locations of vortex pairings may not be the same at different times. Roll up of the mixing layer occurs further upstream in the NFL case than in the NSH case. For both cases, the discrete vortices rotate around each other and merge into larger eddies.

The instability mechanism for the NFL and NSH cases are far more complicated than that for the straight mixing layer. For the NFL case, because the faster stream is on the outside of the curve, the centrifugal instability should be absent based on the Rayleigh circulation criterion. On the contrary, because heavier fluid is on the inside of the curve, the flow is destabilized by the RT effect. For the NSH case, because the slower fluid is on the outside of the curve, the centrifugal instability may destabilize the flow, but the RT effect may stabilize the flow because heavier fluid is on the outside. To measure the instability, we define the turbulent kinetic energy (KE) flux as follows:

$$\mathrm{KE}\,(s) = \int_{R_1}^{R_2} \left[\overline{\rho u_s \left(u_s^2 + u_r^2 \right)} - \overline{\rho u_s} \left(\bar{u}_s^2 + \bar{u}_r^2 \right) \right] \mathrm{d}r \qquad (22)$$

where s is the streamwise location along the centerline; $\bar{()}$ indicates a time-averaged property; u_s and u_r are the streamwise and transverse components of velocity, respectively; and R_1 and R_2 are the radii of the inner and outer curves, respectively. The turbulent kinetic energy fluxes for the NFL and NSH cases and the straight mixing layer are shown in Fig. 4. The statistics for all the cases shown here have reached approximately time-independent states. The statistical data have been gathered over 2 residence time, which is 6–8 times as long as the period of the lowest dominant frequency at far downstream locations; further extensions of the sampling periods do not cause significant changes in the results. Excellent statistically independent

Table 1 Summary of the flow conditions for the straight channel (subscript 1: air; subscript 2: fuel)

	Acceleration	Reaction	u_1, m/s	u_2, m/s	T_1, K	T_2, K	$\frac{dp}{dx}$, atm/m	a_s, $10^3 g's$
Case 1	no	no	50	25	1650	300	0	~0
Case 2	no	yes	50	25	1650	300	0	~0
Case 3	yes	no	50	25	1650	300	−67	257
Case 4	yes	yes	50	25	1650	300	−67	264

Table 2 Summary of the flow conditions for the curved channel

	Reaction	Vel. outside, m/s	Vel. inside, m/s	T outside, K	T inside, K	ρ outside, kg	ρ inside, kg	a_s, $10^3 g's$	a_r, $10^3 g's$
NFL	no	50	25	1650	300	2.19	6.67	~0	1.42
RFL	yes	50	25	1650	300	2.19	6.67	~0	1.65
NSH	no	25	50	300	1650	6.67	2.19	~0	1.57
RSH	yes	25	50	300	1650	6.67	2.19	~0	1.82
NSH-A	no	25	50	300	1650	6.67	2.19	194	354
NFL-A	no	50	25	1650	300	2.19	6.67	149	269
RSH-A	yes	25	50	300	1650	6.67	2.19	194	355
RFL-A	yes	50	25	1650	300	2.19	6.67	149	269

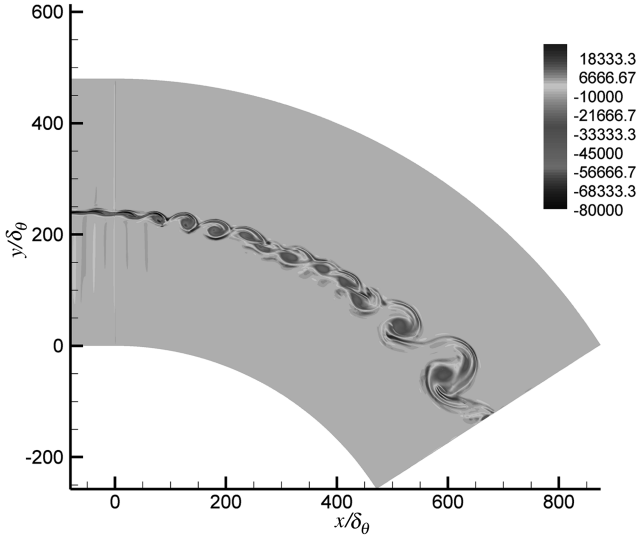

Fig. 2 Instantaneous contours of vorticity (1/s) for the NFL case.

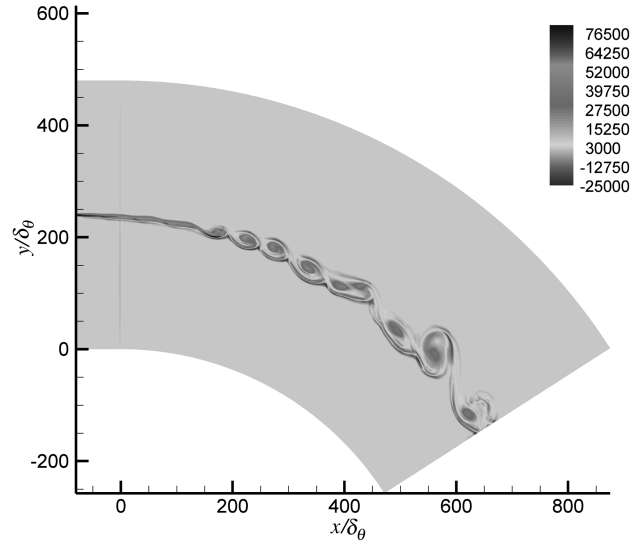

Fig. 3 Instantaneous contours of vorticity (1/s) for the NSH case.

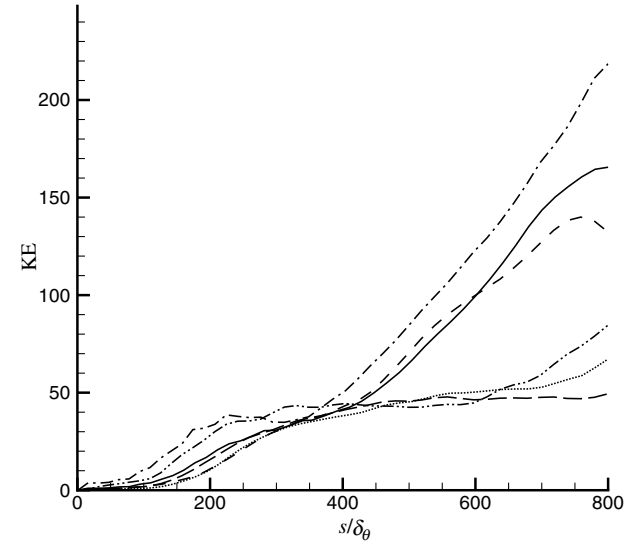

Fig. 4 Turbulent kinetic energy (Joule/sec·m): straight variable ρ case (solid line), NSH case (dashed line), NFL case (dotted-dashed line), straight constant ρ case (dotted line), curved constant ρ case with faster fluid outside (long-dashed line), and curved constant ρ case with faster fluid inside (dashed-double-dotted line).

results are obtained in the upstream positions. The results are roughly statistically time independent in the far downstream positions because of the longer period of the dominant frequency. The results indicate that the NFL case is more unstable than the straight mixing layer. Because the centrifugal instability should be absent in this case, it implies that the RT effect maybe the important destabilizing mechanism in addition to the KH effect. On the other hand, the NSH case is slightly more stable than the straight mixing layer near the exit of the channel. For this case, because the centrifugal instability should destabilize the flow, the stabilizing effect maybe contributed by the RT effect. For the 2-D curved cases, because there are no 3-D instability modes associated with the centrifugal and RT effects, the differences in the instability mechanism between the NFL and NSH cases must be reflected in the 2-D flow profiles. The time-averaged streamwise velocity profiles at a far downstream location of $s = 704\delta_\theta$ for both cases are shown in Fig. 5. The freestream velocities for both cases deviate from the prescribed inlet velocity significantly. Because of the turning, the freestream on the outside experiences a mildly adverse streamwise pressure gradient, whereas the freestream on the inside experiences a mildly favorable streamwise pressure gradient. Consequently, the flow on the outside decelerates, and the flow on the inside accelerates. The difference in the freestream velocities decreases for the NFL case but increases for the NSH case with increasing downstream distance. To gain better understanding on the centrifugal instabilities associated with the velocity profiles and to isolate the effects of the velocity profiles from the RT instability, we have performed computations of straight and curved constant-density mixing layers. The computational domains for the constant-density simulations are identical to those used for the variable-density cases. We have considered two flow configurations for the curved cases; one has the same inflow velocity profile as the NFL case and the other one has the same inflow velocity profile as the NSH case. For both cases, the densities and temperatures at the inlet are uniform across the mixing layers. The Reynolds number (based on ΔU, δ_θ, and the average viscosity) at the inlet is 415 for all cases. The velocity profile for the constant-density case evolves with downstream distance and deviates from the inflow velocity profile significantly. The streamwise velocity profile is similar to that of the corresponding case with variable density as shown in Fig. 5. The turbulent kinetic energies defined in Eq. (22) for the constant-density cases are shown in Fig. 4. For the constant-density cases, the curved case with the faster fluid on the inside is more unstable than the curved case with the faster fluid on the outside, and the straight case is more unstable than the curved case with the faster fluid on the outside. From these results, we deduce that the curved case with the

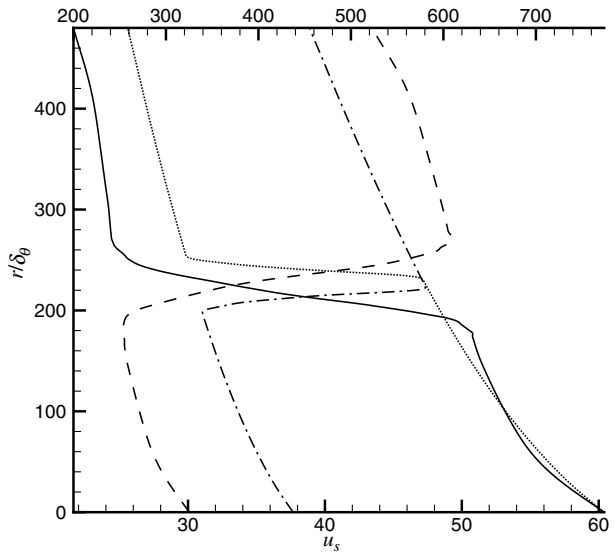

Fig. 5 Time-averaged streamwise velocity profiles (m/s): NSH (solid line) and NFL (dashed-line) cases at $s = 704\delta_\theta$, and NSH-A (dotted line) and NFL-A (dashed-dotted line) cases at $s = 480\delta_\theta$. Lower and upper scales are for the nonaccelerated and accelerated cases, respectively.

faster fluid on the inside is susceptible to centrifugal instability, and the curved case with the faster fluid on the outside is subjected to a stabilizing effect due to the centrifugal force. For the variable-density cases, because the velocity profiles are similar to those for the corresponding constant-density cases, the instability mechanisms associated with the velocity profiles would also be similar. Consequently, we deduce that there is a stabilizing effect associated with the velocity distribution in the NFL case and a destabilizing effect associated with the velocity distribution in the NSH case. On the other hand, the RT effects cannot be extracted by comparing the variable-density case with the corresponding constant-density case. For the variable-density case, the KH instability is enhanced by the density gradient across the mixing layer. That is, even for a nonturning flow without gravity, the density differences are known to affect the KH instability [26]. Therefore, the destabilizing effect of the KH mode in the variable-density case differs from that of the constant-density case and, hence, the RT effects cannot be identified by comparing the overall instabilities. Nevertheless, we expect that the density distribution has a destabilizing effect in the NFL case and a stabilizing effect in the NSH case.

B. Reacting Mixing Layers in a Curved Channel

Reacting mixing layers passing through a curved channel without imposed streamwise pressure gradient are discussed in this section. The flow conditions of the reacting cases are the same as those of the nonreacting cases. Similar to the nonreacting cases, the instantaneous flow patterns are not precisely periodic in time. Because of the chemical reactions, the temperatures of the reacting mixing layers increase tremendously; for both the RFL and RSH cases, the maximum temperatures reach approximately 3250 K. This high temperature has been validated by an adiabatic flame calculation without chemical dissociation. The adiabatic flame temperature for the mixture of fuel (300 K) and air (1650 K) in stoichiometric proportion is 3264 K. Because we do not consider chemical dissociation, the temperature in the simulation would be higher than the practical value. The instantaneous contours of temperature at 3.0 residence time for the RSH and RFL cases are shown in Figs. 6 and 7, respectively. Note that there are some vertical "stripes" near the inlet (they also appear in Figs. 8 and 9). These stripes are numerical noises associated with the inlet boundary conditions but are insignificant and have very little effect on the development of the mixing layer. The flame is defined as the location at which a local maximum of temperature in the transverse direction exists. The flame regions are indicated in the figures by the thin, darkened areas near the centerline of the channel. It is observed that the flames are biased to the hot-air stream as in the straight mixing layer. Roll ups of the mixing layers occur almost immediately

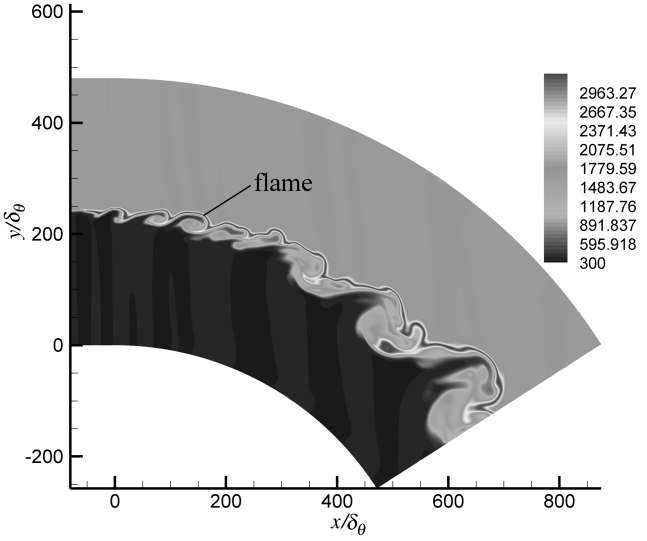

Fig. 7 Instantaneous contours of temperature (K) for the RFL case.

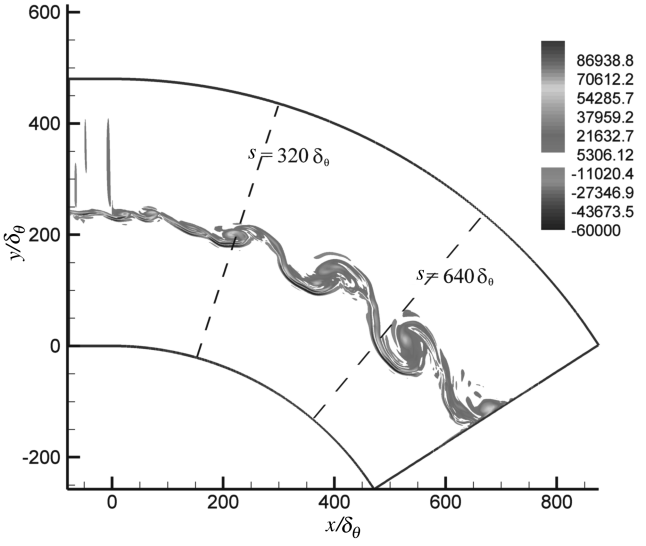

Fig. 8 Instantaneous contours of vorticity (1/s) for the RSH case.

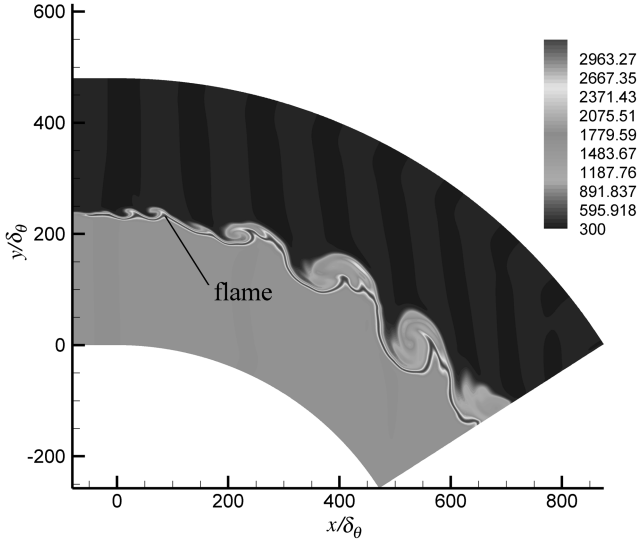

Fig. 6 Instantaneous contours of temperature (K) for the RSH case.

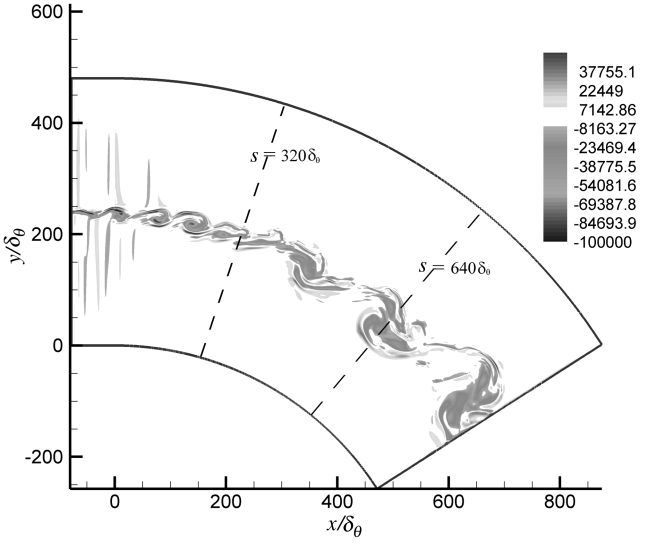

Fig. 9 Instantaneous contours of vorticity (1/s) for the RFL case.

downstream of the inlet. Because of the instability, the ignition regions near the inlet oscillate in the streamwise direction with time. The waviness of the flames originates from the ignition region and grows with downstream distance. Multiple peaks in temperature exist across the mixing layers due to the unsteady vortical motions.

For both curved cases, counter-rotating vortices are generated in the combustion region; this phenomenon is also observed in the straight case and has been discussed in Cheng et al. [16]. In the combustion region, a local minimum in density and a local maximum in streamwise velocity exist. Positive vorticity is generated above the velocity peak, and negative vorticity is generated below the velocity peak. Although there is no imposed pressure gradient in the channel, there is a slightly favorable pressure gradient generated by the channeled flow due to the heat addition, and there are local fluctuations in pressure as well. When the lighter fluids in the combustion region experience a favorable local pressure gradient, they receive relatively larger accelerations than the surrounding fluids, resulting in a local velocity peak. The instantaneous contours of vorticity for the curved reacting cases are shown in Figs. 8 and 9. The development of large coherent structures is clearly seen in the RSH case. For this case, every two or three neighboring vortices usually start pairing around $s = 320\delta_\theta$ and form large coherent structures further downstream. This accounts for the steady growth of the turbulent kinetic energy (discussed in the following paragraph) with increasing downstream distance. On the other hand, the vortices in the RFL case appear to be less coherent than those in the RSH case. For this case, the pairing of vortices is delayed and is not as distinct. The discrete vortices break up into small fragments as they are traveling downstream and usually engage in merging after passing $s = 500\delta_\theta$ (although there is a merging at $s = 460\delta_\theta$ in Fig. 9 at that instant in time). The delay in the formation of large coherent structures is also reflected in the evolution of the turbulent kinetic energy.

To compare the instabilities between the reacting mixing layers, the turbulent kinetic energies defined in Eq. (22) are shown in Fig. 10. Again, the statistical data have been gathered over 2 residence times and have reached approximately statistically independent states for all cases. All of the reacting cases are more unstable than the corresponding nonreacting cases. The destabilizing effect of chemical reaction has been found previously by Cheng et al. [16] in straight mixing layers. Figure 10 shows that the straight mixing layer is more unstable than the two curved mixing layers in most locations except in the region between the inlet and $s = 270\delta_\theta$; this implies that the curvature imposes stabilizing effects on both curved cases. The RFL and RSH cases are subjected to different degrees of stabilization. The RFL case is more unstable than the RSH case near

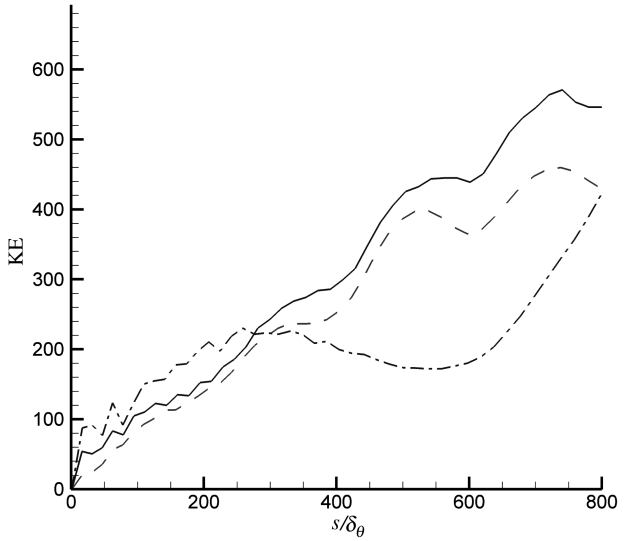

Fig. 10 Turbulent kinetic energy (Joule/sec·m): straight mixing layer (solid line), RSH case (dashed line), and RFL case (dashed-dotted line).

the inlet. However, the instability in the RSH case grows steadily and becomes significantly more unstable in most downstream locations except near the exit of the channel; the steady growth of the turbulent kinetic energy in the RSH case correlates with the formation of large eddies observed from the vorticity field. For the RFL case, the turbulent kinetic energy increases sharply after passing $s = 600\delta_\theta$; this corresponds to the formation of large coherent structures observed from the vorticity field. The instability mechanisms in the curved reacting mixing layers are more complicated due to the chemical reactions and subsequent modifications in velocity, density, and vorticity. The local minimum in density and the local velocity peak can modify the RT instability and the centrifugal instability, respectively. For example, in the RSH case, the lighter products in the combustion region are surrounded by heavier fuel on top and heavier air below. Therefore, there is a destabilizing effect below the density trough but a stabilizing effect above the density trough; this effect is absent in the corresponding nonreacting case because of the monotonic density profile and could be more involved when multiple combustion regions exist across the transverse direction. For the same case, the effects of the velocity profile on the instability are different on different sides of the mixing layer, that is, there is a destabilizing effect on top of the streamwise velocity peak but a stabilizing effect below. The centrifugal effect associated with the velocity profile and the RT effect coexist and can individually impose a stabilizing or destabilizing effect across the turning mixing layer. The combined effects of the velocity profile and the RT mechanism are determined by our nonlinear analysis but the relative importance of each is unclear.

To investigate the chemical conversion rate, the average formation of H_2O along the channel is computed. We define the ratio of mass flow rate of H_2O over the total mass flow rate as follows:

$$\dot{m}_{H_2O} = \frac{\int_0^h \bar{\rho}_{H_2O}\bar{u}\,dy}{\int_0^h \bar{\rho}\,\bar{u}\,dy} \tag{23}$$

where $\bar{()}$ represents a time-averaged quantity and the integrals are evaluated at fixed s locations. Because the products of H_2O and CO_2 are formed, diffused, and advected in stoichiometric proportions, the mass flux calculation in Eq. (23) indicates the amount of product that has been created in the flow up to a specified streamwise position. It can be used as a measure of the efficiency of the chemical conversion process, that is, mixing plus chemical reaction. The results are shown in Fig. 11. The chemical conversion rate for the RFL case is higher than that of the other two cases from the inlet to $s = 780\delta_\theta$, and the straight case is more productive than the RSH case throughout the channel. This result is surprising because the RFL case is indeed the most stable case among the three cases based on the turbulent kinetic energy, and one may think that instability enhances the mixing and chemical reaction rate. To find possible explanations, we examine the flame structures closely and find that smaller wavy structures appear in the RFL case whereas structures with longer wavelengths appear in the RSH case. To examine the waviness quantitatively, we calculate the frequency spectra by Fourier analysis for the three cases and look for the dominant frequency in each case. The frequency can also be expressed in terms of Strouhal number (St). $\mathrm{St} = \omega\delta_\theta/\bar{U}$, where ω is the dominant frequency. For the RFL case, the dominant frequency at $s = 310\delta_\theta$ is 4230 Hz (St = 0.089); for the RSH case and the straight case, the dominant frequencies at $s = 310\delta_\theta$ are approximately 1520 Hz (St = 0.032). The higher frequency in the RFL case correlates with the smaller structures in the upstream portion of the channel. Because the fine structures may enhance the mixing and chemical reaction rate, we believe that those structures account for the increase of the chemical conversion rate.

C. Nonreacting Mixing Layers in a Curved, Converging–Diverging Channel

Nonreacting mixing layers passing through the curved channel with a converging–diverging cross-sectional area in the z direction are studied in this section. The inflow conditions for all cases are the same as the corresponding nonaccelerating cases. For convenience,

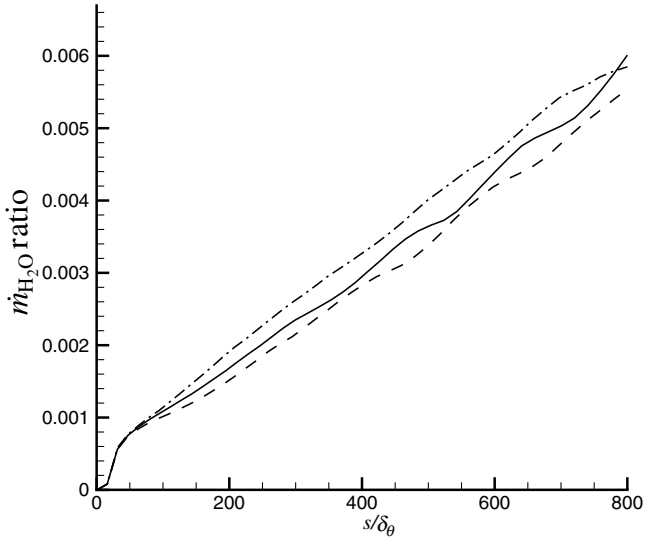

Fig. 11 Ratio of mass flow rate of H_2O: straight mixing layer (solid line), RSH case (dashed line), and RFL case (dashed-dotted line).

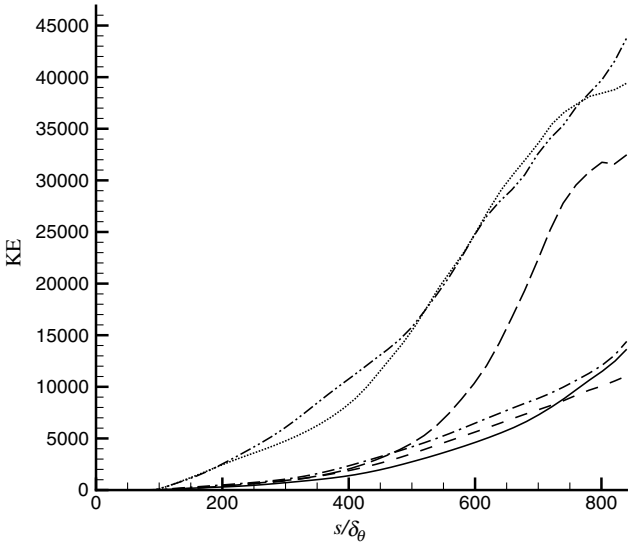

Fig. 12 Turbulent kinetic energies (Joule/sec·m) for the accelerating cases: straight nonreacting case (solid line), NSH-A case (dashed line), NFL-A case (dashed-dotted line), straight reacting case (dotted line), RSH-A case (long-dashed line), and RFL-A case (dashed-double-dotted line).

we describe the cases with and without imposed streamwise acceleration as the accelerating and nonaccelerating cases, respectively. The accelerating cases that correspond to the NSH and NFL cases are described as NSH-A and NFL-A, respectively. The converging–diverging channel is designed such that the contraction ratio along the centerline is the same as the contraction ratio in the converging–diverging straight channel. Also, the contraction ratio does not vary in the radial direction. Similar to the nonaccelerating cases, the flowfields are also not precisely periodic in time. The sampling period of the statistics is about 10 times as long as the period of the lowest dominant frequency far downstream, and statistically independent results are obtained.

The imposed streamwise pressure gradient accelerates the flow tremendously. The mixing layers accelerate from low subsonic speed near the inlet to supersonic speed near the exit for all cases. For the curved mixing layers, the flows on the outside of the curve are subjected to smaller favorable streamwise pressure gradients, whereas the flows on the inside of the curve are subjected to larger favorable streamwise pressure gradients. This variation of streamwise pressure gradient in the transverse direction is attributed to the turning of the channel and the variation of the converging–diverging rate of the channel width. Because the channel width (θ) is constant in the transverse direction, the magnitude of the rate of change of θ with respect to the streamwise location is higher on the inside due to shorter length but lower on the outside due to longer length. Because of the nonuniform streamwise pressure gradients, the freestream velocities differ significantly in the different cases. The time-averaged streamwise velocities at $s = 480\delta_\theta$ are shown in Fig. 5. For the NSH-A case, the freestream velocity is much higher on the inside because of the larger favorable pressure gradient and lower density. Also, the difference in the freestream velocities increases significantly with increasing downstream distance. For the NFL-A case, the freestream velocities are close to each other because the lighter stream is subjected to a smaller favorable pressure gradient and the heavier stream is subjected to a larger favorable pressure gradient. For this case, the difference in the freestream velocities is relatively insensitive to the downstream distance. Although the velocity profiles differ significantly in different cases, the Mach number profiles remain similar. For both cases, the Mach numbers of the freestreams at the exit are approximately 1.9 on the inside and 1.0 on the outside.

For the nonreacting NSH-A and NFL-A cases, the imposed streamwise pressure gradient shows a strong stabilizing effect. In general, roll ups of the mixing layers are much delayed; waviness starts to develop near the exit but the mixing layers do not break up into discrete vortices as in the nonaccelerating cases. The instabilities of the NSH-A and NFL-A cases and the straight case are shown in Fig. 12. The amplitudes of the turbulent kinetic energy for the accelerating cases are approximately 2 orders of magnitude larger than those for the nonaccelerating ones, but the accelerating cases appear to be much more stable. This phenomenon has been observed in the straight mixing layers [16]; the instability for the accelerating flow is more energetic in the absolute sense, but the accelerating flow is more stable because the growth of the instability is outbalanced by the faster increasing mean kinetic energy due to the strong acceleration. We have computed the ratios of the turbulent kinetic energy to the mean kinetic energy for each curved case and its corresponding straight case. The results reveal that the nonaccelerating cases are more unstable than the accelerating counterparts in terms of the ratio of the turbulent kinetic energy to the mean kinetic energy. The trend in the instabilities for the accelerating cases is similar to that for the nonaccelerating ones. The NFL-A case is more unstable than the NSH-A case throughout the channel, and the straight case is more unstable than the NSH-A case but more stable than the NFL-A case near the exit. The similar trend is probably attributed to the similarities in the mean flow profiles and the instability mechanisms with the nonaccelerating cases (see Fig. 5). The streamwise acceleration causes a large increase in the streamwise velocity and the magnitude of vorticity but does not introduce new structures, such as a local velocity peak or a local density peak. We believe that the stabilizing effect is attributed to the reduced residence time so that the instability has less time to develop.

D. Reacting Mixing Layers in a Curved, Converging–Diverging Channel

Reacting mixing layers passing through the curved channel with a converging–diverging cross-sectional area in the z direction are investigated in this section. The inflow conditions for the accelerating cases are the same as those for the corresponding nonaccelerating cases. The accelerating and reacting cases that correspond to the RSH and RFL cases are described as RSH-A and RFL-A, respectively. Similar to the nonreacting, accelerating cases, the flows accelerate from low subsonic speed at the inlet to supersonic speed at the exit. For both cases, the freestream Mach numbers at the exit are approximately 1.85 on the inside and 1.0 on the outside. Because of the strong streamwise accelerations, large local velocity peaks (much more pronounced than those in the nonaccelerating cases) are generated in the low-density combustion regions for both the RSH-A and RFL-A cases. The velocity peaks increase with increasing downstream distance, so that the differences between the peak velocities and the freestreams become larger. In

each of those cases, positive vorticity is generated above the velocity peak in the combustion zone and negative vorticity is generated underneath; the strengths of the vorticities of both signs increase with increasing downstream distance. The instantaneous contours of vorticity for the RSH-A (at 1.75 residence time) and RFL-A (at 1.84 residence time) cases are shown in Figs. 13 and 14, respectively. Note that the flowfields are not precisely periodic in time, and the locations of roll ups vary with time too. The labeled thin layers near the centerline of the channel are the vorticity layers of opposite signs. For both cases, the mixing layers are quite steady in the upstream locations before roll ups of the vorticity layers occur. For the RFL-A case, roll up of the vorticity layer usually occurs around $s = 510\delta_\theta$. This location is further downstream than that of the nonaccelerating RFL case, but further upstream than that of the nonreacting but accelerating NFL-A case. For the RSH-A case, roll up of the vorticity layer is delayed compared with the RFL-A case; it usually occurs around $s = 640\delta_\theta$. This location is further downstream than that of the nonaccelerating RSH case, but further upstream than that of the nonreacting but accelerating NSH-A case.

To investigate the instabilities further, the turbulent kinetic energies shown in Fig. 12 are examined. The turbulent kinetic energies for the accelerating and reacting cases are 3–4 times as large as those for the accelerating but nonreacting cases. It once again shows that the chemical reactions destabilize the mixing layers. To compare the instabilities between the accelerating flow and the nonaccelerating flow, it is more appropriate to examine the ratio of the turbulent kinetic energy to the mean kinetic energy, because the mean kinetic energy is increasing in the accelerating flow. We have found that all the accelerating and reacting cases are more stable than the corresponding nonaccelerating but reacting cases in terms of the ratio of turbulent kinetic energy to the mean kinetic energy. In the accelerating mixing layer, the disturbances do not grow as fast as the mean kinetic energy, and so the flow is stabilized by the streamwise acceleration.

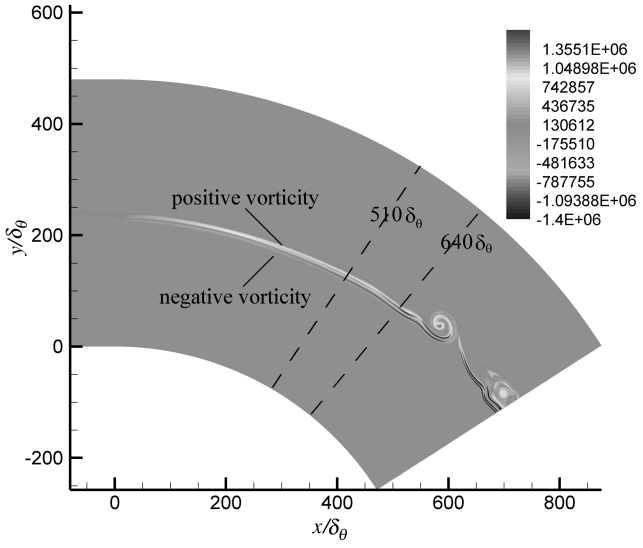

Fig. 13 Instantaneous contours of vorticity (1/s) for the RSH-A case.

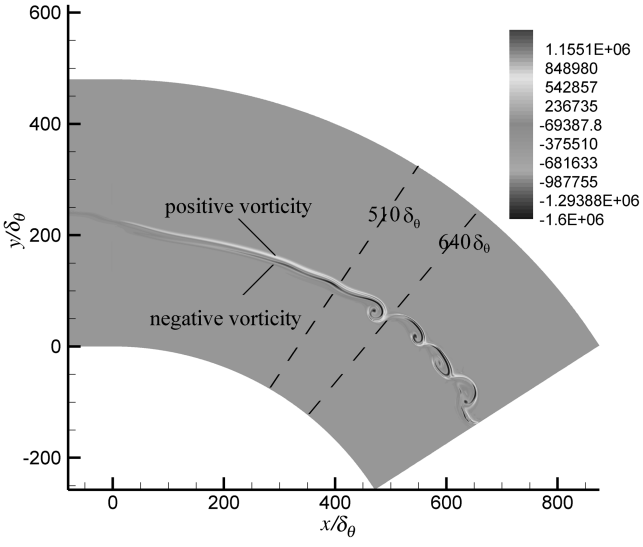

Fig. 14 Instantaneous contours of vorticity (1/s) for the RFL-A case.

Figure 12 shows that the RFL-A case is more unstable than the RSH-A case and slightly more unstable than the straight case. In the laminar region, the dominant vorticity in the RFL-A case is approximately equal in magnitude to that of the RSH-A case in the far upstream locations; however, the dominant vorticity in the RFL-A case increases more rapidly and becomes larger further downstream. The larger dominant vorticity may contribute to the earlier roll up of the mixing layer in the RFL-A case and may enhance instability. To investigate the development of the vorticity, we examine the dominant terms in the vorticity equation. The 2-D vorticity equation is shown as follows:

$$\frac{\mathrm{D}\omega_z}{\mathrm{D}t} = \frac{1}{\rho^2}\nabla\rho \times \nabla p - \omega_z \nabla \cdot \mathbf{u} + \text{viscous term} \qquad (24)$$

Because the vorticity (ω_z) is normal to the velocity field, the vortex stretching term vanishes in Eq. (24). The dominant terms in generating vorticity are the baroclinic torque [the first term on the right-hand side of Eq. (24)] and the divergence effect [the second term on the right-hand side of Eq. (24) without the negative sign]. The viscous term is much smaller than the other terms, and so it is neglected in the analysis. For each case, the baroclinic term and the divergence term have the same signs as the local vorticity, and the baroclinic term is approximately two times as large as the divergence term. The baroclinic term always intensifies the vorticity, but the divergence term always weakens the vorticity. Because the baroclinic term is always larger than the divergence term, the net effect causes the magnitudes of vorticities of both signs to increase. For the RFL-A case, the vorticity generating terms become increasingly larger than those of the RSH-A case with increasing downstream distance so that the rate of production of the dominant vorticity is larger. This accounts for the larger dominant vorticity in the RFL-A case. The typical profiles for the baroclinic and divergence terms are shown in Fig. 15, at $s = 340\delta_\theta$. The data are taken at 1.75 and 1.84 residence times for the RFL-A and RSH-A cases, respectively. Note that at that location the mixing layers are quite laminar, and so the results vary very slightly with time. The dominant baroclinic term in the RFL-A case is approximately 11% larger than that of the RSH-A case, and the dominant divergence term in the RFL-A case is marginally larger than that of the RSH-A case. The rate of production of the dominant vorticity in the RFL-A case is approximately 18% larger than that of the RSH-A case.

The chemical reactions and the streamwise pressure gradients cause an interesting development of flame structures not seen in the nonaccelerating but reacting cases. The instantaneous contours of temperature for the RSH-A (at 1.75 residence time) and RFL-A (at 1.84 residence time) cases are shown in Figs. 16 and 17, respectively. In each figure, the flame corresponds to the high-temperature region indicated by the thin dark region near the centerline of the channel, and the peak temperature drops with increasing streamwise distance due to the thermal expansion under acceleration. For both cases, the flames appear to be laminar and quite steady in time in the upstream regions. The laminar regions for both cases cover at least 50% of the total length of the channel, followed by the development of waviness and roll ups of the flames. The roll-up locations are consistent with those found in the vorticity contours. As the vortical structures propagate downstream, the flames continue to curl and are stretched simultaneously due to the acceleration and eventually tear into fragments. In this paper, flame tearing is defined as the condition in which the local peak temperature drops below 2200 K. In the nonaccelerating, reacting cases, flame tearing does not occur; the

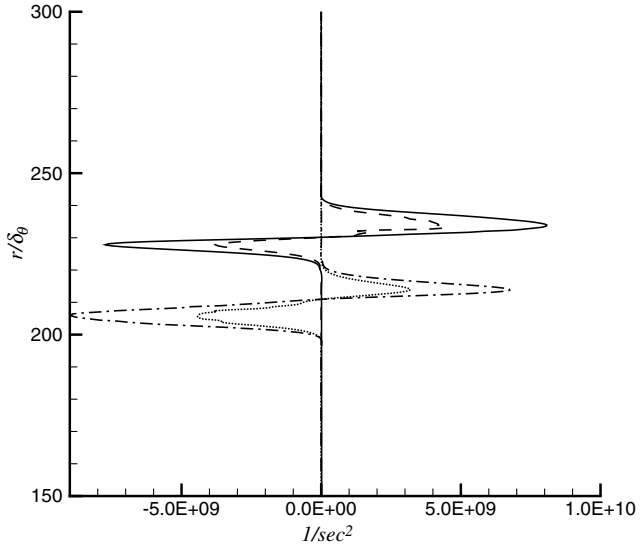

Fig. 15 Baroclinic and divergence terms ($1/s^2$) for the RFL-A and RSH-A cases: baroclinic term for RSH-A case (solid line), divergence term for RSH-A case (dashed line), baroclinic term for RFL-A case (dashed-dotted line), and divergence term for RFL-A case (dotted line).

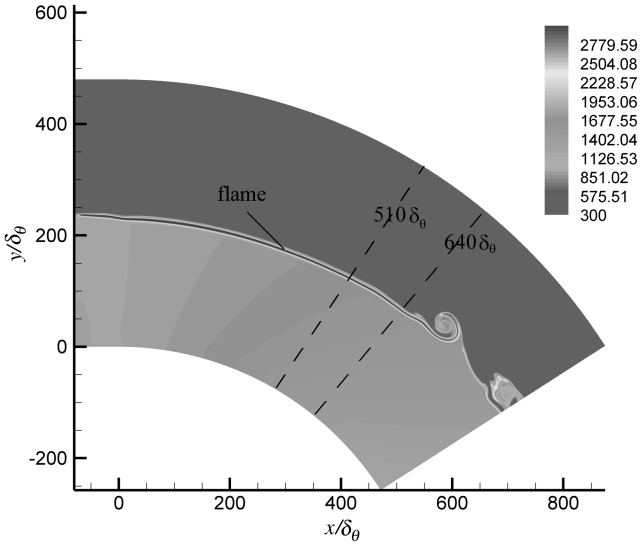

Fig. 16 Instantaneous contours of temperature (K) for the RSH-A case.

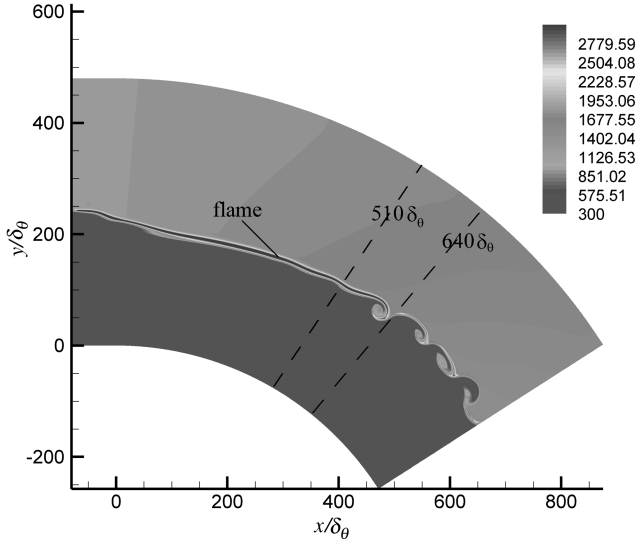

Fig. 17 Instantaneous contours of temperature (K) for the RFL-A case.

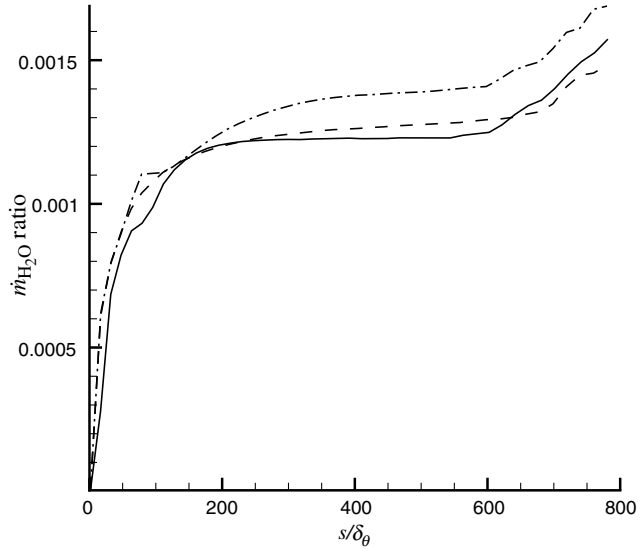

Fig. 18 Ratio of mass flow rate of H_2O: straight mixing layer (solid line), RSH-A case (dashed line), and RFL-A case (dashed-dotted line).

flames are always continuous and the peak temperature is relatively constant with downstream distance.

The mass fluxes of product H_2O defined in Eq. (23) for the accelerating cases are compared in Fig. 18. The RFL-A case is the most productive one among the three cases; the RSH-A case is slightly more productive than the straight case initially but is overtaken by the straight case near the end of the channel. The growths of the chemical conversion rate show very similar trends for the three cases. Note that the trends are quite different from those for the nonaccelerating, reacting mixing layers in which the chemical conversion rates increase almost linearly with increasing downstream distance. For the accelerating cases, the chemical conversion rates increase sharply from the inlet to $s = 150\delta_\theta$. Then, the chemical conversion rates increase slowly further downstream but start to rise again significantly at certain far downstream locations. For the RFL-A and straight cases, the chemical conversion rates start to surge significantly after passing $s = 600\delta_\theta$; for the RSH-A case, the chemical conversion rate starts to increase significantly again at $s = 680\delta_\theta$. Comparing Fig. 18 with the vorticity contours, we observe that the regions in which the chemical conversion rates increase slowly correspond to the laminar regions with little waviness. This implies that mixing may be inhibited in the laminar, accelerating regions so that the chemical reactions are retarded. The moderate increases in the chemical conversion rates far downstream occur in the regions dominated by the formation of large eddies. The large vortical structures promote mixing and, hence, the chemical reactions are enhanced. Because the RFL-A case is more unstable than the other two cases, it is not surprising that it has the largest chemical conversion rate.

V. Conclusions

Numerical simulations on curved mixing layers with or without chemical reactions have been performed. The effects of the transverse and streamwise pressure gradients and the chemical conversion rate are investigated. The flows considered are of negligible gravity force, and so the RT instability is caused by the centrifugal force. For the nonreacting mixing layers without imposed streamwise pressure gradient, the curvature destabilizes the NFL case (faster and lighter fluid on the outside) but stabilizes the NSH case (slower and heavier fluid on the outside). We believe that the RT mechanism contributes to the destabilizing effect in the NFL case and the stabilizing effect in the NSH case. Although the flows are two-dimensional so that no 3-D unstable modes arise from the centrifugal and RT instabilities, the effects of the centrifugal force are still present through the modifications of the flow profiles. For the reacting cases without imposed streamwise pressure gradient, both

the RFL and RSH cases are more unstable than the corresponding nonreacting cases, but are more stable than the straight reacting mixing layer. The destabilizing effect due to the chemical reaction is consistent with the findings in the straight reacting mixing layers [16]. Pronounced overshoot in the streamwise velocity and the undershoot in density across the transverse direction contribute to the destabilizing effect. The stabilizing effect due to the turning is not immediately clear. We have found that there can be multiple streamwise velocity and density peaks across the transverse direction in both curved cases. The centrifugal effect associated with the velocity profile and the RT mechanism can individually impose a stabilizing effect on one side of the peak but a destabilizing effect on the other side. Although we can determine the combined effects of both mechanisms, the relative importance of each remains unclear.

The curved mixing layers with imposed streamwise accelerations with or without chemical reactions are more stable than their nonaccelerating counterparts. The roll ups of the mixing layers with imposed streamwise accelerations are much delayed, but the turbulent kinetic energies are much larger than those of the corresponding cases without streamwise accelerations. The flows are stabilized because the increase in the mean kinetic energy due to the streamwise acceleration is more dominant, so that the disturbances relative to the mean flow become less significant. This stabilizing effect is confirmed by evaluating the ratio for turbulent kinetic energy (absolute turbulent kinetic energy normalized by the mean kinetic energy) and is consistent with the finding in the straight mixing layers. For the nonreacting cases, the turning slightly destabilizes the NFL-A case but stabilizes the NSH-A case. This trend is similar to that in the cases without imposed streamwise acceleration. Although the streamwise acceleration intensifies the vorticity tremendously, the flow profiles remain similar to those without streamwise acceleration, so that the instability mechanisms are also similar. The reacting mixing layers with imposed streamwise accelerations show that the chemical reactions destabilize the flows again. This destabilizing effect again indicates the large overshoot in streamwise velocity and the undershoot in density enhance instability. The turning slightly destabilizes the RFL-A case but stabilizes the RSH-A case. The destabilizing effect is probably due to the larger dominant vorticity in the RFL-A case. Because the RFL-A case is more unstable, the mixing and chemical conversion rate are enhanced.

Finally, the present numerical simulation could be extended to three dimensions. In a 3-D simulation, the spanwise variations of the flowfields will be solved for and the geometry of the converging–diverging channel could be modeled more accurately. Also, the 3-D instability modes associated with the centrifugal and RT instabilities can be captured. The formation and evolution of the streamwise vortical structures in an accelerating, reacting mixing layer would be a very interesting subject for future studies.

Acknowledgments

The authors wish to thank Air Force Office of Scientific Research (AFOSR) for the partial support of this research with Julian Tishkoff as the Scientific Officer.

References

[1] Sirignano, W. A., and Liu, F., "Performance Increases for Gas-Turbine Engines Through Combustion Inside the Turbine," *Journal of Propulsion and Power*, Vol. 15, No. 1, 1999, pp. 111–118.

[2] Liu, F., and Sirignano, W. A., "Turbojet and Turbofan Engine Performance Increases Through Turbine Burners," *Journal of Propulsion and Power*, Vol. 17, No. 3, 2001, pp. 695–705.

[3] Sirignano, W. A., and Kim, I., "Diffusion Flame in a Two-Dimensional, Accelerating Mixing Layer," *Physics of Fluids*, Vol. 9, No. 9, 1997, pp. 2617–2630. doi:10.1063/1.869378

[4] Fang, X., Liu, F., and Sirignano, W. A., "Ignition and Flame Studies for an Accelerating Transonic Mixing Layer," *Journal of Propulsion and Power*, Vol. 17, No. 5, 2001, pp. 1058–1066.

[5] Mehring, C., Liu, F., and Sirignano, W. A., "Ignition and Flame Studies for an Accelerating Transonic Turbulent Mixing Layer," AIAA Paper 01-0190, 2001.

[6] Cai, J., Icoz, O., Liu, F., and Sirignano, W. A., "Ignition and Flame Studies for Turbulent Transonic Mixing Layer in a Curved Duct Flow," AIAA Paper 01-0180, 2001.

[7] Ho, C. M., and Huerre, P., "Perturbed Free Shear Layers," *Annual Review of Fluid Mechanics*, Vol. 16, Jan. 1984, pp. 365–424. doi:10.1146/annurev.fl.16.010184.002053

[8] Winant, C. D., and Browand, F. K., "Vortex Pairing: The Mechanism of Turbulent Mixing Layer Growth at Moderate Reynolds Number," *Journal of Fluid Mechanics*, Vol. 63, No. 2, 1974, pp. 237–255. doi:10.1017/S0022112074001121

[9] Rogers, M. M., and Moser, R. D., "The Three-Dimensional Evolution of a Plane Mixing Layer: The Kelvin–Helmholtz Rollup," *Journal of Fluid Mechanics*, Vol. 243, 1992, pp. 183–226. doi:10.1017/S0022112092002696

[10] Moser, R. D., and Rogers, M. M., "The Three-Dimensional Evolution of a Plane Mixing Layer: Pairing and Transition to Turbulence," *Journal of Fluid Mechanics*, Vol. 247, 1993, pp. 275–320. doi:10.1017/S0022112093000473

[11] Drazin, P. G., and Reid, W. H., *Hydrodynamic Stability*, Cambridge Univ. Press, Cambridge, England, U.K., 1981.

[12] Liou, W. W., "Linear Stability of Curved Free Shear Layers," *Physics of Fluids*, Vol. 6, No. 2, 1994, pp. 541–549. doi:10.1063/1.868350

[13] Zhuang, M., "The Effects of Curvature on Wake-Dominated Incompressible Free Shear Layers," *Physics of Fluids*, Vol. 11, No. 10, 1999, pp. 3106–3115. doi:10.1063/1.870168

[14] Shin, D. S., and Ferziger, J. H., "Linear Stability of the Reacting Mixing Layer," *AIAA Journal*, Vol. 29, No. 10, 1991, pp. 1634–1642.

[15] Shin, D. S., and Ferziger, J. H., "Linear Stability of the Compressible Reacting Mixing Layer," *AIAA Journal*, Vol. 31, No. 4, 1993, pp. 678–685.

[16] Cheng, F., Sirignano, W. A., and Liu, F., "Nonpremixed Combustion in an Accelerating Transonic Flow Undergoing Transition," *AIAA Journal*, Vol. 45, No. 12, 2007, pp. 2935–2948. doi:10.2514/1.31146

[17] Westbrook, C. K., and Dryer, F. L., "Chemical Kinetic Modeling of Hydrocarbon Combustion," *Progress in Combustion Science*, Vol. 10, 1984, pp. 1–57.

[18] White, F. M., *Viscous Fluid Flow*, 2nd ed., McGraw–Hill, New York, 1991.

[19] Tannehill, J., Anderson, D. A., and Pletcher, R. H., *Computational Fluid Mechanics and Heat Transfer*, 2nd ed., Talyor and Franics, Washington, D.C., 1997.

[20] Steger, J. L., and Warming, R. F., "Flux Vector Splitting of the Inviscid Gasdynamic Equations with Application to Finite-Difference Methods," *Journal of Computational Physics*, Vol. 40, No. 2, April 1981, pp. 263–293. doi:10.1016/0021-9991(81)90210-2

[21] Hirsch, C., *Numerical Computation of Internal and External Flows*, Vol. 2, Computational Methods for Inviscid and Viscous Flows, Wiley, New York, 1990.

[22] Davis, R. W., and Moore, E. F., "A Numerical Study of Vortex Merging in Mixing Layers," *Physics of Fluids*, Vol. 28, No. 6, 1985, pp. 1626–1635. doi:10.1063/1.864954

[23] Poinsot, T. J., and Lele, S. K., "Boundary Conditions for Direct Simulations of Compressible Viscous Flows," *Journal of Computational Physics*, Vol. 101, No. 1, July 1992, pp. 104–129. doi:10.1016/0021-9991(92)90046-2

[24] Grinstein, F. F., "Open Boundary Conditions in the Simulation of Subsonic Turbulent Shear Flows," *Journal of Computational Physics*, Vol. 115, No. 1, Nov. 1994, pp. 43–55. doi:10.1006/jcph.1994.1177

[25] Grinstein, F. F., Oran, E. S., and Boris, J. P., "Pressure Field, Feedback, and Global Instabilities of Subsonic Spatially Developing Mixing Layers," *Physics of Fluids A*, Vol. 3, No. 10, 1991, pp. 2401–2409. doi:10.1063/1.858178

[26] Groppengiesser, H., "Study on the Stability of Boundary Layers in Compressible Fluids," NASA TTF-12, 1970.

T. Jackson
Associate Editor